GEOPHYSICS, VOL. 75, NO. 1 (JANUARY-FEBRUARY 2010); P. T1–T8, 7 FIGS.
10.1190/1.3273868

Seismic modeling and analysis of a prototype heated nuclear waste storage tunnel, Yucca Mountain, Nevada

Steven Smith[1] and Roel Snieder[1]

ABSTRACT

We have developed seismic velocity models for the heated rock surrounding a tunnel in Yucca Mountain tuff and compared the results with field data obtained at the Yucca Mountain drift scale test (DST) facility from 1998 to 2002. During that time, the tunnel was heated to replicate the effects of long-term storage of decaying nuclear waste and to study the effects of extreme temperatures on the surrounding rock and groundwater flow. Our velocity models are based on borehole temperature data, thermal models, and laboratory measurements on granite. Comparisons between field and synthetic seismograms show that superheating the rock around the tunnel causes thermally induced variations in P- and S-wave arrival-time separation. Barring out-of-plane reflections, 2D spectral element waveform modeling in the source plane consistently replicates seismic receiver waveforms and classic behavior of pulses reflected from cylinders. Our models constrain the in situ $V^{-1}dV/dT$ velocity/temperature derivative of the tuff to be approximately -0.5% per 100°C. This velocity change is consistent with thermally induced wavespeed changes in dry rock samples and is lower than expected for water-to-steam conversion in saturated rock. We infer that velocity changes are controlled by thermal expansion and fracturing. Additionally, we have developed an improved method for monitoring tunnel conditions that uses waves diffracted around the tunnel in the region of changing velocity.

INTRODUCTION

The Yucca Mountain complex, located 90 miles northwest of Las Vegas, Nevada, U.S.A., is America's prototype facility for the long-term storage of high-level nuclear waste from reactors and decommissioned atomic weapons. Radioactive decay of deposited waste is expected to superheat the storage tunnels, and environmental monitoring during this heating may determine if damage occurs to the surrounding rock. There is concern that such damage may allow groundwater to enter and exit, compromise waste containers, and carry contaminants downward to regional aquifers (Spycher et al., 2003). Here, we show that superheating the rock around the tunnel causes thermally induced variations in P- and S-wave arrival-time separation. Inverting the P-S separation and velocity field provides insight regarding the spatial extent and degree of change in the surrounding rock caused by excessive heat.

A small-scale replica of a full-size storage tunnel was heated and monitored from 1998 to 2004 (Yucca Mountain heated drift-scale test [DST]) (TRW, 1998; Tsang et al., 1999; Rutqvist, 2004). This test tunnel is located within a large block of tuff (welded volcanic ash) halfway between the surface and water table and hundreds of meters from major bounding fault planes (Day et al., 1998). The tunnel was heated to approximately 200°C over two years and maintained at that temperature for the remaining two years. One of two sets of heating elements is a group of faux waste canisters located along the tunnel axis, with a second set of wing heaters extending 15 m into the rock on either side (Figure 1a). The entire system was monitored simultaneously for hydrological, chemical, seismic, and similar indications of environmental changes. Figure 1b shows an end-on view of the intended nuclear waste storage cylinders and hypothetical groundwater saturation (Spycher et al., 2003). Any groundwater near the high-temperature wall of the tunnel is expected to completely dry out (near ellipse), whereas groundwater at a distance from the wall may undergo a water-to-steam phase transition (far ellipse).

Most current rock-property studies tend to focus on sedimentary rocks critical to petroleum exploration and production (Ibrahim and Keller, 1981; Sayers and Chopra, 2009). However, simultaneous high-temperature and pressure wavespeed measurements of igneous rocks similar to Yucca Mountain tuff have been obtained (Bayuk and Tedeyev, 1974; Spencer and Nur, 1976; Kern, 1978). Based on these

Presented at the 78th Annual International Meeting, SEG.
Manuscript received by the Editor 23 June 2008; revised manuscript received 24 July 2009; published online 19 January 2010; corrected version published online 1 March 2010.
[1]Colorado School of Mines, Geophysics Department, Center for Wave Phenomena, Golden, Colorado, U.S.A. E-mail: stesmith@mines.edu; rsnieder@mines.edu.

studies, we know that P- and S-wave velocities are sensitive to thermal changes, and we observed such effects in data gathered around the test tunnel by others (discussed in the next section). Consequently, we hypothesized that these changing wavespeeds result from thermal effects and from changing groundwater conditions. Therefore, our objective was to determine how P and S velocity perturbations and P-S arrival time separations could delineate the amount and spatial extent of thermally induced velocity change in the rock, with the hope of inferring whether a distribution of groundwater was present, changing, and potentially affecting tunnel conditions.

We used both field and modeling approaches. We processed and analyzed seismic data collected during the second through fourth years of the 1998–2002 heating cycle (Rutledge, 2006, personal communication). The data consisted of calibration shots recorded on a receiver array intended to passively detect acoustic emissions associated with stressed rock (Kaiser effect) (Rutledge et al., 2003; Lehtonen, 2005; Grêt et al., 2006) (Figure 1b). The calibration shots were to verify functionality of the array after it failed during the first year of heating. Our velocity models are physical analogs derived by fitting polynomials to laboratory measurements of wavespeeds in dry granite samples (Carmichael, 1989; Grêt et al., 2006). We used on-site temperature borehole measurements, published thermal models (Rutqvist, 2004), and laboratory data to model spatial distributions of temperature-based velocity changes around the tunnel. We adjust these models to the in situ background velocities of tuff

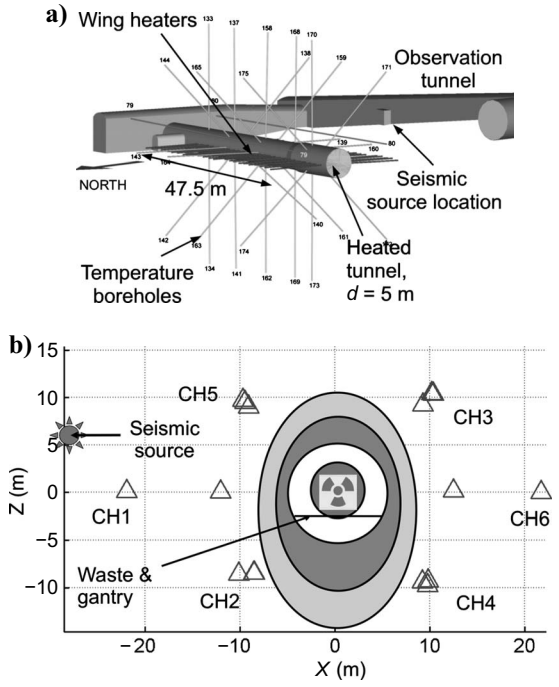

Figure 1. (a) A 3D visualization of the Yucca Mountain DST tunnel modified from Rutqvist (2004) via Bechtel SAIC Company (2002), showing experimental tunnel with temperature-monitoring boreholes and wing heaters. Seismic source (sledgehammer) location is in the adjoining observation tunnel. (b) Seismic array receiver locations (triangles) distributed along the length of the heated tunnel (end-on view). Labeled receivers used are in the plane of the source perpendicular to the tunnel (CH1–CH6). Shaded regions around emplaced nuclear waste storage canister (center) approximate the hypothetical groundwater dryout (near ellipse) and water-steam/dryout phase transition (far ellipse) following Spycher (2003).

using arrival-time lags for relative source-receiver distances.

The field data shows an increasing separation between P- and S-wave arrivals with increasing temperature (Figure 2). The P-S separation did not change once the target temperature in the tunnel was achieved. These results helped form the comparisons we sought. We show that granite-based velocity modeling constrains in situ velocity changes at the tunnel wall to approximately -0.5% per $100\,^{\circ}\mathrm{C}$. Further, velocity-model parametrization shows the inversion process could serve as a seismic thermometer for the tunnel interior. We discuss how a radial distribution of receivers can exploit diffracted waves propagating near the tunnel in the region of temperature variation. This array could be used to monitor changes in the surrounding rock caused by radioactive heating.

FIELD DATA PROCESSING

A joint effort by Los Alamos, Sandia, Lawrence Livermore, and Lawrence Berkeley National Laboratories collected seismic data about the 47.5-m-long, 5-m-diameter tunnel using receiver locations shown by triangles in Figure 1b. The entire array is emplaced along the length of the tunnel, but we focus our analysis on the six receiver channels, labeled CH1–CH6 (Figure 1b). These receivers are colocated with the source in a plane perpendicular to the tunnel axis. Each receiver is a single-component instrument assumed to be aligned along the axis of its radially oriented borehole and of like electrical polarity. The seismic source was a sledgehammer strike perpendicular to the tunnel wall located in the adjoining instrumentation drift tunnel 28 m away and 6 m above the axis of the experimental drift, with a useful bandwidth of approximately 2 kHz (Figure 1a) (TRW, 1998; Rutledge, 2006). No attempt was made to implement a control mechanism for consistent source energy output during data collection, and no trigger information exists with the data set.

We processed the data to remove coherent band-limited noise and spurious samples (deglitching). An example receiver gather is shown in Figure 2. The time interval between successive events is not uniform, with calibration shots recorded at random intervals between 21 December 1998 and 14 January 2002 (inclusive). These dates are indicated by square data markers in tunnel-wall temperature data (Figure 3a). Waveforms recorded on the same day were stacked to improve signal-to-noise ratio (S/N). Because the raw data lack a trigger signal, waveforms are aligned by first breaks for correlation analysis. The data demonstrate an increasing P-S separation that occurs up to approximately two years into the experiment. Around that date, temperature stabilizes to within $20\,^{\circ}\mathrm{C}$ of the $200\,^{\circ}\mathrm{C}$ target temperature, and the P-S separation remains roughly constant. We observed this P-S separation trend to varying extents in all of the processed receiver gathers, and we hypothesized that the trend is caused by changing wavespeeds in the neighborhood of the tunnel, resulting from thermal effects and changing groundwater saturation as described in Ide (1937), Bayuk and Tedeyev (1974), Spencer and Nur (1976), Kern (1978), and Grêt et al. (2006).

VELOCITY MODELING

We constructed temperature-dependent velocity models for the 2D elastic waveform modeling used to describe wavespeed changes in the surrounding rock. We assume the Yucca Mountain tuff to be isotropic with a density of $2.359\ \mathrm{g/cm^3}$, as measured from a borehole depth of 1000 ft (300 m) (Martin et al., 1994). Temperature

measurements from boreholes extending above and below the tunnel were used to constrain ambient velocities and velocity variations for modeling (Rutqvist, 2004). The data provide temperature as a function of radial distance from the tunnel wall at 12-month intervals. This allows the extrapolation of a continuous temperature profile at the tunnel wall over the duration of the experiment (Figure 3a).

The minor axis of an elliptical thermal/velocity transition zone caused by the core and wing heaters (Figure 3b) was computed by interpolating the 12-month borehole-temperature-data surface at calibration shot temperatures indicated in Figure 3a. Within this elliptical zone, temperature and velocity measurements transition between values at the heated wall and ambient conditions in undisturbed rock. Ellipticity of this zone in the velocity models was based on the ellipticity of a modeled temperature distribution around the tunnel and wing heaters after 12 months of operation, as proposed by Rutqvist (2004). We assumed that this ellipticity remains constant for all temperatures, resulting in a growing elliptical thermal velocity perturbation directly correlated with temperature values at the tunnel wall.

Wavespeed as a function of temperature from two separate sets of measurements on granite was used as a physical analog to generate two separate models of $V_P(T)$ and $V_S(T)$ for Yucca Mountain tuff (Figure 3c and d). Granite was used to model tuff because both are igneous rocks with 65–75% quartz content (Carmichael, 1989; Grêt et al., 2006). This allows us to constrain the slope of V_P and V_P/V_S as a function of temperature using realistic bounds. We assumed grain size was not a primary velocity control because fracturing occurs around and through grains at sufficiently high temperatures and pressures (Bayuk and Tedeyev, 1974; Batzle et al., 1980).

Generally, igneous rocks measured under high temperatures and pressures experience increasing velocities with increasing pressure. They experience decreasing velocities with increasing temperature, with a critical temperature where the slope of the velocity curve changes (see Figure 3d) (Grêt et al., 2006). This change in $V(T)$ slope is attributed to thermal expansion of matrix components and associated microfracturing (Bayuk and Tedeyev, 1974; Spencer and Nur, 1976; Kern, 1978; Grêt et al., 2006).

The $V_P(T)$ curves from the second set of granite data shown by the solid circles in Figure 3d demonstrate an incomplete heating/cooling hysteresis cycle associated with these principles. A single cycle is indicated by directional arrows. Branch 1 shows decreasing velocity with increasing temperature. Branch 2 shows decreases in velocity above the critical temperature in which thermal expansion and microfracturing occur. Grêt et al. (2006) notes that this branch is also associated with increasing acoustic emissions (Kaiser effect). Branch 3 is the cooling branch of the cycle, with a slope similar to heating branch 1 and velocity returning to a lower value at the initial temperature. Open squares indicate a second heating and cooling cycle in which the previous maximum temperature has not been exceeded and additional damage does not occur to the matrix.

Examples of cycles for temperatures exceeding the previous critical temperature on samples at atmospheric pressure are given by Ide (1937). Similar velocity/temperature and stress/strain hysteresis data have been observed by Bayuk and Tedeyev, (1974) and Batzle et al. (1980), respectively. High confining pressures can limit expansion and fracturing to the matrix (Bayuk and Tedeyev, 1974); therefore, we limited our use of velocity measurements to an extension of branch 1 in Figure 3d when generating our second tuff model.

Because the seismic data lacks a trigger, relative arrival-time lags for a set of receivers were measured to determine the in situ ambient velocity of Yucca Mountain tuff. Early calibration shot records and receivers with minimal transgressions of heated regions by the source/receiver path were used to minimize thermal interference. Knowing the relative differences in path length and time lags, an average background velocity of 3600 m/s was established. This value agrees well with ambient velocities of Yucca Mountain Topopha tuff of approximately 15% porosity as given by New England Research (2007) and Indian Springs tuff from the Mines Commonground Database (Batzle and Scales, 2008).

The granite data shown in Figure 3c and d were fit with polynomials, and coefficients were adjusted to move the curves downward so that the data matches the in situ ambient velocity of the tuff at the ambient rock temperature. Both curves retain the slope and V_P/V_S ratio of the granite analogs, resulting in two individual velocity versus temperature models for tuff (Figure 3e and f). These models have -0.5% and -2.5% P-wave velocity slopes with respect to ambient velocities over a 100°C temperature variation. Because -2.5% velocity slope granite data in Figure 3d consisted only of V_P measure-

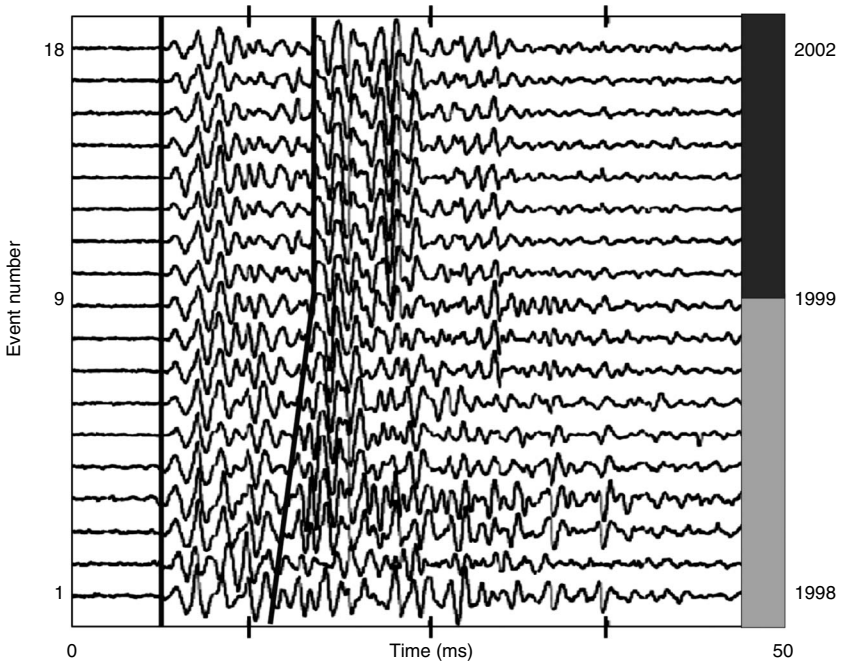

Figure 2. Example receiver gather for instrument with (X,Z) coordinate of CH3 (Figure 1b). Data are aligned to first breaks and arranged chronologically from bottom to top (years on right). Calibration events were recorded at nonuniform intervals between 21 December 1998 and 14 January 2002 (inclusive). Light color bar on right side of data indicates event numbers in which the tunnel temperature was increasing. Dark color bar on right side of data indicates event numbers in which temperature was approximately constant near 200°C. Guidelines highlight a trend of increasing P-S arrival separation.

ments, P/S velocity ratios of the −0.5% velocity slope granite data in Figure 3c were used to generate S-wave velocities for the −2.5% velocity slope tuff model. An example compressional velocity model for the initial event at a temperature of approximately 135°C is shown in Figure 4. Note that the seismic calibration shots neither begin at ambient temperature/velocity conditions nor continue into the

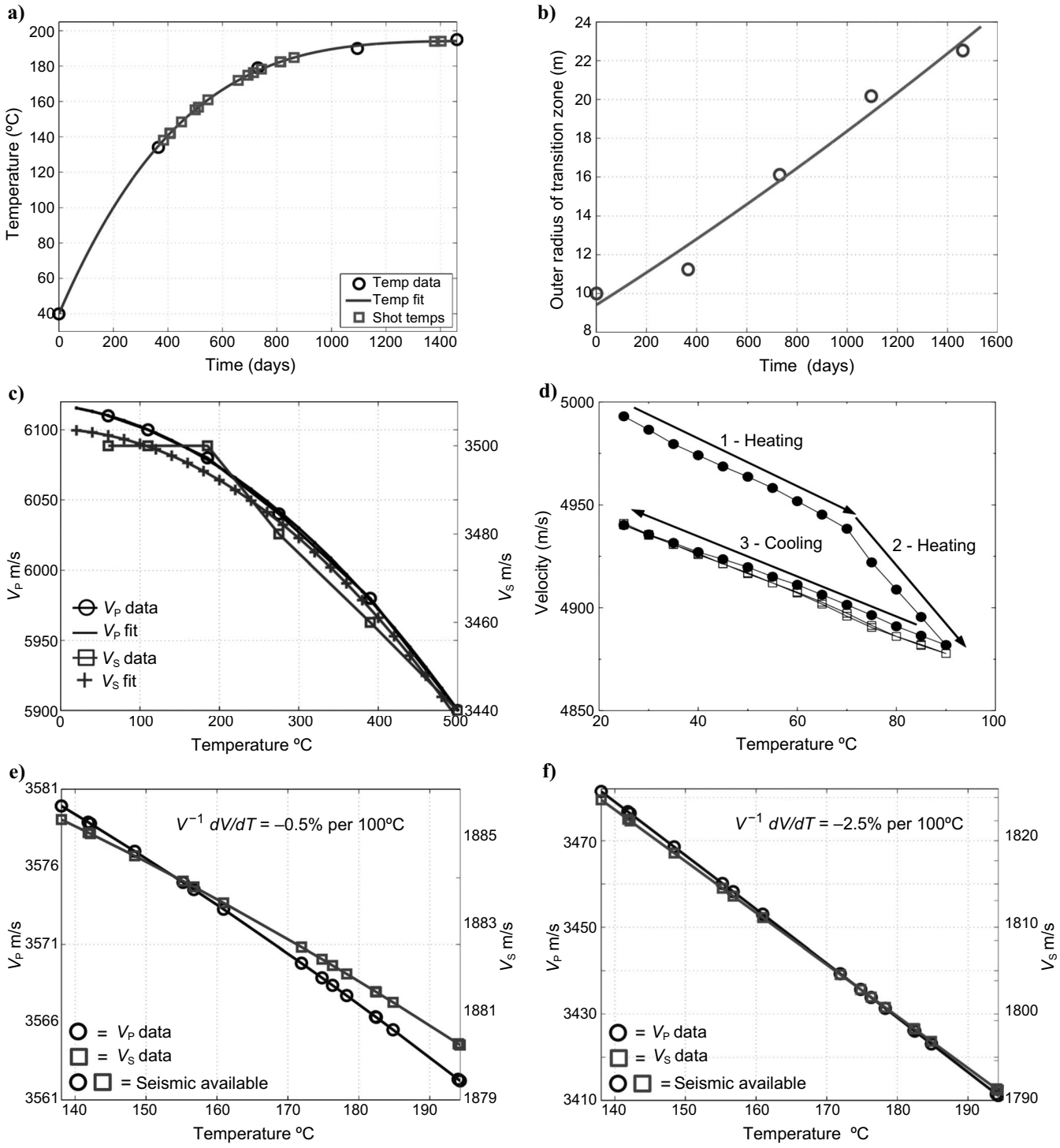

Figure 3. Data related to $V_{P,S}(T)$ model parametrization as detailed in the text. (a) Tunnel-wall temperature. (b) Minor (vertical) axis of thermal transition zone. (c and d) Granite wavespeed data from Carmichael (1989) and Grêt et al. (2006), respectively. (e, f) Extrapolated tuff wavespeed models having − 0.5% and − 2.5% slopes per 100°C with respect to ambient velocity. Squares in (a) and circles on lines in (e) and (f) indicate days when seismic data were available.

cooling phase when the heaters were shut down, prohibiting an in situ measurement of a temperature-velocity hysteresis similar to that of Ide (1937), Bayuk and Tedeyev (1974), or Grêt et al. (2006) (Figure 3d).

MODEL/DATA COMPARISON

We synthesized seismic signals with each velocity/temperature distribution for kinematic comparison with preprocessed field data. Model waveforms were generated using SEM2DPACK spectral-element software (Ampuero, 2007), a 2D package that limits analysis to receivers that are located approximately in the plane of the seismic source, perpendicular to the tunnel. Spectral-element modeling (Komatitsch and Vilotte, 1998; Komatitsch and Tromp, 1999) uses a variational integral formulation and interpolating polynomials across computational mesh elements to solve for displacement. It does not suffer from the dispersion effects and numerical instabilities in finite-element and finite-difference algorithms, associated with mesh spacing or interpolation errors (Virieux, 1986; Levander, 1988; Muir et al., 1992; Juhlin, 1995). Potential but less useful alternative methods of numerical modeling include smoothing of interfaces and rotated staggered grids, which require a high number of points per wavelength (Saenger et al., 2000; Bohlen and Saenger, 2006).

The bandwidth of spectral-element modeling is 2 kHz, and field data are zero-phase low-passed to this bandwidth. The input source for synthetic seismograms is a Ricker wavelet of matching bandwidth. Minor variations between model and field waveforms exist because of reflection and scattering by the connecting access tunnel. Because we seek a simple kinematic comparison, no adjustments were made to account for differences in geometric spreading in two and three dimensions. Generally, both sets of waveforms exhibit structure composed of incident, reflected, and converted waves consistent with numerical simulations by Liu et al. (2000).

Good agreement between modeled and field data are shown in Figure 5. The data shown include all calibration events for a receiver with a source-receiver path crossing most of the thermal transition zone (CH4) and include P- and S-wave arrivals. Data are aligned to the first break of the P-waves, but because of shadowing and interference, they have a significantly lower P/S amplitude for this receiver than that of Figure 2. Figure 6a and b zooms in on the alignment of S-wave arrivals for the −0.5% and −2.5% per 100°C tuff models, respectively. Field data waveforms were preprocessed as described above and aligned to the first break of the model data for each event. Again, we focus on the P-S separation as shown in Figure 2 because acceptable models should account for this trend. The vertical line across the S-wave arrivals serves as a reference of constant traveltime.

Acceptable agreement between modeled and field waveforms is

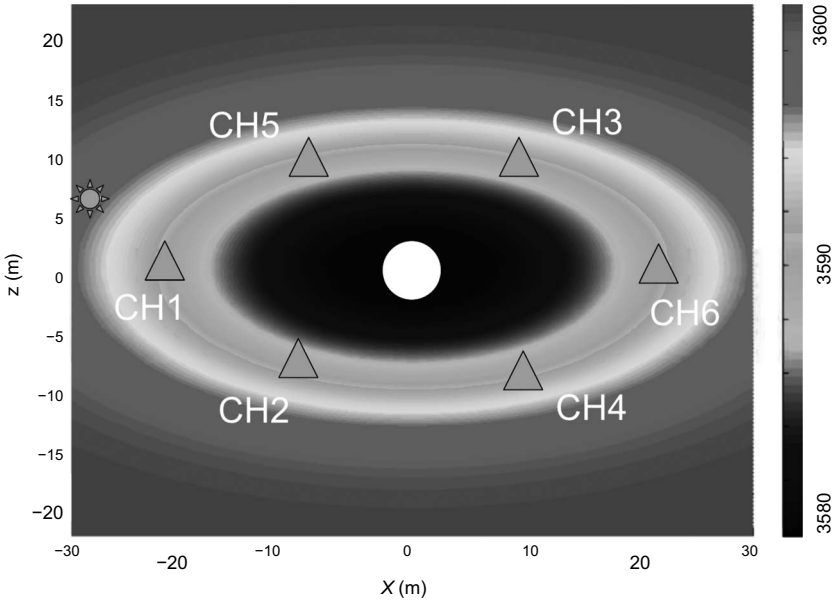

Figure 4. Example initial P-wave velocity model (m/s) (383 days from initiation of heating) derived from granite/tuff data in Figure 3c and e. Elliptical geometry caused by the presence of wing heaters is similar to thermal models shown by Rutqvist (2004). Source and receivers in the source-plane perpendicular to the tunnel are shown, as in Figure 1b.

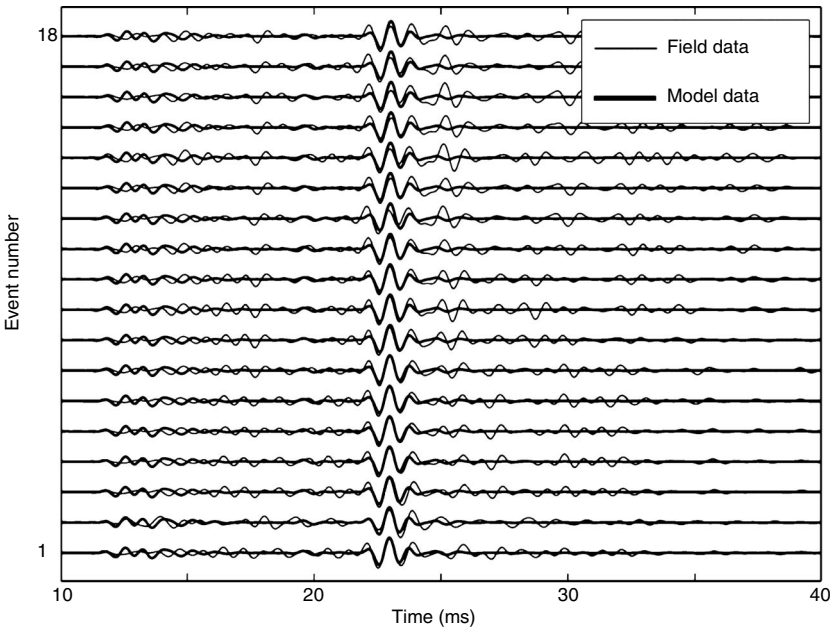

Figure 5. Comparison of waveforms recorded at CH4 (Figure 4) showing model (heavy) versus field data (thin) for a temperature derivative of −0.5%/100°C with respect to ambient temperature and velocity. Calibration-shot event numbers on the vertical axis increase at nonuniform intervals with time and tunnel-wall temperature, beginning on 3 December 1998 and concluding 14 January 2002. Data are aligned to first break of compressional waves to correct for lack of trigger, as in Figure 2. Because of interference effects and location of this receiver in the tunnel shadow zone, the ratio of P to S amplitudes is lower than other receivers not in the shadow zone. P-S arrival separation of the model data closely matches the field data.

achieved for models with a −0.5% per 100°C velocity change, as shown in Figure 6a, whereas the 2.5% per 100°C velocity change shown in Figure 6b is inconsistent with the observed waveforms. Unacceptable velocity models (Figure 6b) possess incorrect P- and S-wave arrival times, but all data are aligned to the first break of the field data P-waves, so only changes in the S-wave arrival are displayed. For cases where the slope of the $V(T)$ models lies between −0.5% and −2.5% per 100°C, we assume a smooth progression between models. The reproduced P-S separation trends in the models based on temperatures measured at the tunnel wall show that subsurface changes are detectable and tunnel-wall temperature can be quantified using seismic data.

From a monitoring perspective, we want to understand changes in the surrounding rock using the seismic data. Velocity changes in the acceptable models are consistent with dry laboratory samples. In some cases, thermally induced velocity changes in igneous rocks can be as high as −2%/100°C (Guéguen and Palciauskas, 1994). These values exceed the approximately −20 m/s (−0.55%/100°C) maximum velocity change in the acceptable models of Figure 3e by at least 3.6 times. Gassmann fluid substitution (Wang, 2001; Mavko et al., 2003; Smith et al., 2004) using laboratory data obtained from tuff cores acquired 1000 ft (300 m) below Yucca Mountain (Martin et al., 1994; Christianson et al., 2004) for water-saturated rock with fractional gas saturation (<0.001%, i.e., approaching $T = 100$°C) and water-to-steam bulk modulus changes ($\Delta T \geq 100$°C) (Wang, 2001) gives P- and S-wave velocity changes approaching 200 m/s and 125 m/s, respectively (5.5% and 3.5% of background V_P). These values exceed the maximum velocity change in the acceptable models by a factor of about 6.25. If significant amounts of water were present in the region around the tunnel, we would expect more significant changes in the velocity (Bayuk and Tedeyev, 1974).

Total bulk modulus is also controlled by thermal expansion and change in fracture pore space (Spencer and Nur, 1976). Total porosity is the initial pore space plus any space caused by fracturing (fracture porosity). Mechanisms for altering fracture porosity include changes to the matrix properties with temperature, deviatoric stress from tunnel emplacement, and compression by the overlying mass column. Thermal expansion can fracture rocks of differing mineral content and increase fracture porosity. Deviatoric stresses can increase fracture porosity by forcing open existing fractures or compressing small fragments in existing fractures (Batzle et al., 1980). Occurrence of fracturing is supported by localization of microseisms around the tunnel (Rutledge et al., 2003). These circumstances imply that velocity changes observed in the seismic data, within the region subtended by the seismic array, are governed primarily by a change in the properties of the rock matrix and fracture porosity changes.

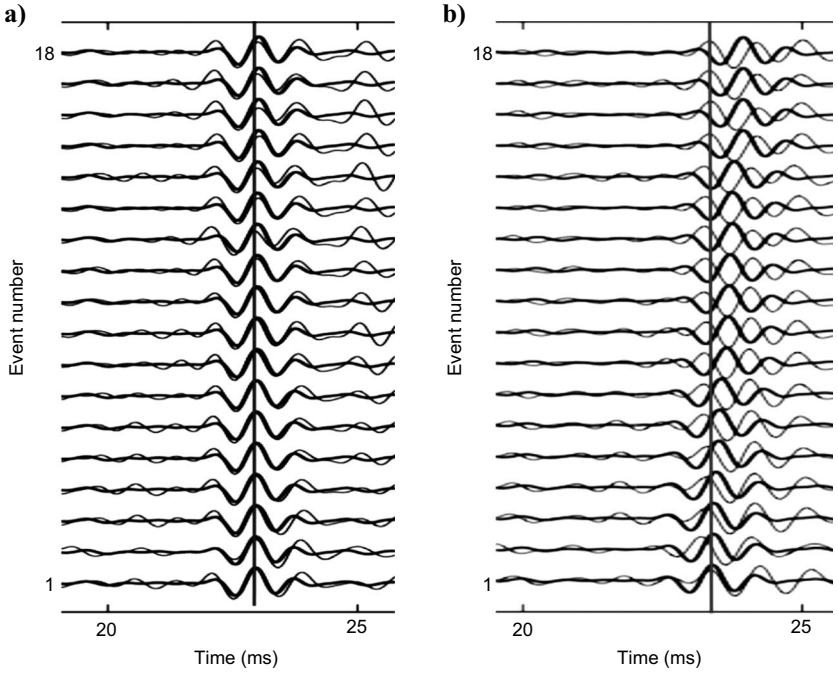

Figure 6. Close-ups of CH4 shear-wave arrival shot gathers for extrapolated tuff $V_{P,S}(T)$ models of Figure 3e and f having (a) −0.5% per 100°C and (b) −2.5% per 100°C velocity changes, respectively. Plot style follows previous figure. Model waveforms are darker heavier traces. Data are from CH 4, located below tunnel opposite from source. Shear-wave arrivals show good agreement for models based on −0.5% per 100°C slope. All field and model waveforms in (b) arrive at later times than (a). This is because field data waveforms, lacking a trigger, are aligned to the first breaks of model waveforms, and the velocity/temperature derivative is greater for waveforms in (b).

In addition to constraints on the velocity, numerical modeling shows the presence of a diffracted wave (Franz wave) propagating in the shadow zone of the tunnel. This wavefront is oriented normal to the tunnel and propagates around its surface. It is described analytically by Gilbert and Knopoff (1959) and observed experimentally by Neubauer and Dragonette (1970). The wave can be clearly seen propagating over the upper surface of the tunnel in the modeled data of Figure 7a, extending toward the receiver CH3 in Figure 1b. A complementary wave propagates in the opposite direction under the tunnel but with attenuated amplitude because of interference caused by asymmetry of the tunnel system.

Comparison of numerical modeling to the seismic data indicates potential candidates for Franz-wave arrivals, but poor S/N in the field data precludes definite identification or analysis of these waves. Low Franz-wave S/N occurs because the receiver array did not include elements located sufficiently close to the thermal transition zone. Franz-wave sensitivity to velocity changes near the tunnel suggests that future monitoring of rock conditions can be achieved by observing transit times of the Franz wave around the surface of the tunnel or differential arrival times of the curved wavefront by a linear array extending radially from the tunnel wall. Suggested array improvements for this purpose are shown in Figure 7b.

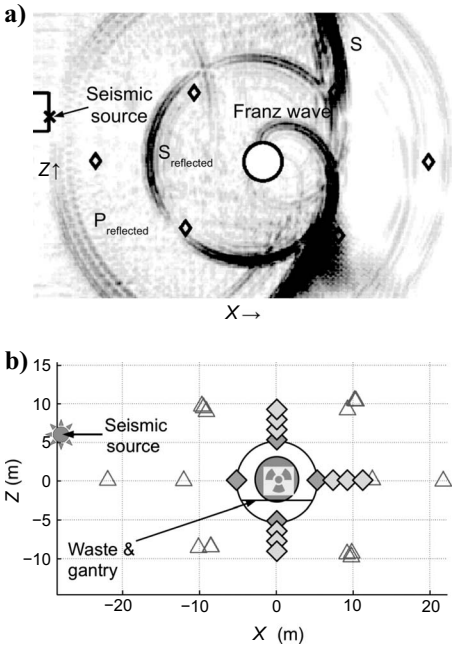

Figure 7. A snapshot of the numerically modeled wavefield shows a Franz (diffracted) wave propagating over the tunnel crown. Lines of constant phase are normal to the tunnel near the wall, having a velocity-dependent increase in curvature with increasing radial distance. Because the Franz wave propagates about the tunnel in the velocity/temperature transition zone, measurement of its arrival times as a function of distance from the tunnel wall is a potential tool for monitoring tunnel conditions. (b) Suggested improvements to the existing array consist of surface and radially emplaced receivers (diamonds) to measure passage and curvature of Franz wavefronts about the tunnel.

CONCLUSIONS

Processing seismic data from the Yucca Mountain heated DST of 1998–2002 shows clear changes in P-S wavelet separation as a function of time and temperature. We developed temperature-based velocity models for Yucca Mountain tuff derived from thermal borehole data, thermal simulations, and laboratory measurements of temperature-dependent velocity in granite. These models were used to synthesize seismograms at receivers in plane with the seismic source; simulated wavefields compare well with known theoretical and experimental wavefields around cylinders.

Kinematic comparison of field and synthetic waveforms shows that well-constrained velocity models replicate the P-S arrival separation as a function of temperature. Therefore, changes in the surrounding rock can be detected seismically, and temperature values at the tunnel wall can be inferred from the data. Good agreement with wavespeed models having a $-0.5\,\%\,/\,100\,^{\circ}\mathrm{C}$ velocity change is consistent with dry sample data from laboratory measurements. However, this velocity change is low relative to expected values from literature or expected velocity change caused by a water-to-steam conversion as computed with the Gassmann equation. Therefore, we infer velocity changes to be controlled by thermal expansion and dynamic fracture porosity. Localizations of induced seismicity support thermal expansion and fracturing as the primary velocity control.

Traveltime perturbations caused by thermally induced wavespeed changes may be applied as a secondary or remote method for measuring temperature changes inside the tunnel. Unfortunately, the current data set suffers from irregular shot intervals, high levels of noise, and an array configuration not intended for sampling the region of temperature change. Thus, as shown here, this process requires that one know velocity/temperature relations with good accuracy. Diffracted phases propagating in the shadow zone of the tunnel should exhibit greatest sensitivity to changes in temperature and velocity near the tunnel and will be useful monitoring tools if a linear array of receivers extending outward from the tunnel wall is installed.

Future experiments of this type would benefit from a dense arrangement of receivers in the region of temperature change. Additional receivers located near the source, and far from the tunnel, would improve estimations of source signature and background velocities. A proper trigger mechanism is desireable to improve precision. Seismic control data collected prior to heating and data collected in the cooling phase should be analyzed to monitor velocity hysteresis cycles indicating potential change or stabilization of the surrounding rock.

ACKNOWLEDGMENTS

This work has been conducted as part of U.S. Department of Energy grant DE-FG02-06ER15778. The authors thank Jim Ruttledge (LANL) for access to Yucca Mountain DST seismic data. We also acknowledge Jean-Paul Ampuero (ETH/CalTech), Mike Batzle (CSM/CRA), Jyoti Behura (CSM/CWP), Thomas Bohlen (TU Bergakademie Freiberg), Dave Hale (CSM/CWP), Matt Haney (Sandia NL), Yaoguo Li (CSM/CGEM), Ernie Majer (LBNL), John Peterson (LBNL), Jeff Roberts (LLNL), Jim Rutledge (LANL), Jonny Rutqvist (LBNL), Erik Saenger (Fachrichtung Geophysik, Freie Universitaet Berlin), John Stockwell (CSM/CWP), Jeroen Tromp (Princeton), Kenneth Hurst-Williams (LBNL), Shuki Ronen (CGG Veritas), and Sergio Grion (CGG Veritas) for information, discussions, and suggestions.

REFERENCES

Ampuero, J., 2007, SEM2DPACK: A spectral element method for 2D wave propagation and fracture dynamics, with emphasis on computational seismology and earthquake source dynamics: ETH Zürich (Swiss Federal Institute of Technology), Institute of Geophysics, Seismology and Geodynamics Group, v2.2.9 edition, accessed 7 August 2009;. http://sourceforge.net/projects/sem2d/.

Batzle, M., and J. Scales, 2008, Mines common ground database: Colorado School of Mines, accessed 7 August 2009; http://commonground.mines.edu/.

Batzle, M. L., G. Simmons, and R. W. Sigfried, 1980, Microcrack closure in rocks under stress: Direct observation: Journal of Geophysical Research, **85**, 7072–7090.

Bayuk, Y. I., and R. V. Tedeyev, 1974, The longitudinal wave velocity in rock samples under the simultaneous action of high pressure and temperature: Izvestiya, Physics of the Solid Earth, **10**, 521–526.

Bechtel SAIC, 2002, Thermal testing measurements report: National Labs Report ANL-NBS-HS-000041 REV 00, internal report.

Bohlen, T., and E. Saenger, 2006, Accuracy of heterogeneous staggered-grid finite-difference modeling of Rayleigh waves: Geophysics, **71**, no. 4, T109–T115.

Carmichael, R. S., 1989, CRC practical handbook of physical properties of rocks and minerals: CRC Press.

Christianson, M. C., M. P. Board, and D. B. Rigby, 2004, UDEC simulation of triaxial testing of lithophysal tuff: U.S. Department of Energy Technical Report DC 42815, MOL.20041020.0028.

Day, W. C., R. P. Dickerson, C. J. Potter, D. S. Sweetkind, C. A. S. Juan, R. M. Drake II, and C. J. Fridrich, 1998, Bedrock geologic map of the Yucca Mountain area, Nye County, Nevada: U.S. Geological Survey Report I-2627.

Gilbert, F., and L. Knopoff, 1959, Scattering of impulsive elastic waves by a

rigid cylinder: Journal of the Acoustical Society of America, **31**, 1169–1175.
Grêt, A., R. Snieder, and J. Scales, 2006, Time-lapse monitoring of rock properties with coda wave interferometry: Journal of Geophysical Research, **111**, doi: 10.1029/2004JB003354.
Guéguen, Y., and V. Palciauskas, 1994, Introduction to the physics of rocks: Princeton University Press.
Ibrahim, A. W., and G. V. Keller, 1981, Seismic velocities and electrical resistivity of recent volcanics and their dependence on porosity, temperature, and water saturation: Geophysics, **46**, 1415–1422.
Ide, J. M., 1937, The velocity of sound in rocks and glasses as a function of temperature: Journal of Geology, **45**, 689–716.
Juhlin, C., 1995, Finite-difference elastic wave propagation in 2-D heterogeneous transversely isotropic media: Geophysical Prospecting, **43**, 843–858.
Kern, H., 1978, The effect of high temperature and high confining pressure on compressional wave velocities in quartz-bearing and quartz-free igneous and metamorphic rocks: Tectonophysics, **44**, 185–203.
Komatitsch, D., and J. Tromp, 1999, Introduction to the spectral element method for three-dimensional seismic wave propagation: Geophysical Journal International, **139**, 806–822.
Komatitsch, D., and J. P. Vilotte, 1998, The spectral element method: An efficient tool to simulate the seismic response of 2D and 3D geological structures: Bulletin of the Seismological Society of America, **88**, 368–392.
Lehtonen, A., 2005, Evaluation of rock stress estimation by the Kaiser effect: Posiva Oy, Working Report 2005-67.
Levander, A., 1988, Fourth-order finite-difference P-SV seismograms: Geophysics, **53**, 1425–1436.
Liu, Y., R. Wu, and C. Ying, 2000, Scattering of elastic waves by an elastic or viscoelastic cylinder: Geophysical Journal International, **142**, 439–460.
Martin, R. J., R. H. Price, P. J. Boyd, and J. S. Noel, 1994, Bulk and mechanical properties of the paintbrush tuff recovered from borehole USW NRG-6: Data Report: Sandia National Laboratories Report SAND93-4020.
Mavko, G., T. Mukerji, and J. Dvorkin, 2003, The rock physics handbook: Cambridge University Press.
Muir, F., J. Dellinger, J. Etgen, and D. Nichols, 1992, Short note: Modeling elastic fields across irregular boundaries: Geophysics, **57**, 1189–1193.
Neubauer, W., and L. Dragonette, 1970, Observation of waves radiated from circular cylinders caused by an incident pulse: Journal of the Acoustical Society of America, **48**, 1135–1149.
New England Research, 2007, Bulk and mechanical properties of paintbrush tuff from Yucca Mountain, NV: New England Research Technical Report, accessed 7 August 2009; http://nersolutions.com/pdf/NER_tn_paintbrush_tuff.pdf.
Rutledge, J., C. Roe, J. Peterson, and E. Majer, 2003, Relocation of Yucca Mountain induced microseismicity: Los Alamos National Laboratory Technical Report EES-11 Geophysics.
Rutqvist, J., 2004, Drift scale THM model: U.S. Office of Civilian Radioactive Waste Management Technical Report MDL-NBS-HS-000017 REV00.
Saenger, E., N. Gold, and S. Shapiro, 2000, Modeling the propagation of elastic waves using a modified finite-difference grid: Wave Motion, **31**, 77–92.
Sayers, C., and S. Chopra, 2009, Introduction to the special section — Rock physics: The Leading Edge, **28**, no. 1, 15–16.
Smith, T. M., C. H. Sondergeld, and C. S. Rai, 2004, Gassman fluid substitutions: A tutorial: Geophysics, **68**, 430–440.
Spencer, J. W., and A. M. Nur, 1976, The effects of pressure, temperature, and pore water on velocities in Westerly granite: Journal of Geophysical Research, **81**, 899–904.
Spycher, N., E. Sonnenthal, and J. Apps, 2003, Fluid flow and reactive transport around potential nuclear waste emplacement tunnels at Yucca Mountain, Nevada: Journal of Contaminant Hydrology, **62–63**, 653–673.
TRW, Inc., 1998, Drift scale test as-built report: Technical Report BAB000000-01717-5700-00003 REV 01.
Tsang, Y. W., J. Apps, J. T. Berkholzer, J. E. Peterson, E. Sonnenthal, N. Spycher, and K. H. Williams, 1999, Yucca Mountain drift scale test progress report: Lawrence Berkley National Laboratory Technical Report LBNL-42538.
Virieux, J., 1986, P-SV wave propagation in heterogeneous media: Velocity stress finite-difference method: Geophysics, **51**, 889–901.
Wang, Z., 2001, Y2K tutorial: Fundamentals of seismic rock physics: Geophysics, **66**, 398–412.